OPEN

Molecular Psychiatry (2018) 23, 199–210

www.nature.com/mp

ORIGINAL ARTICLE

A novel mechanism of memory loss in Alzheimer's disease mice via the degeneration of entorhinal–CA1 synapses

X Yang[1,2,6], C Yao[1,2,6], T Tian[1,2,6], X Li[1,2,6], H Yan[1,2], J Wu[1,2], H Li[1,2], L Pei[2,3], D Liu[2,4], Q Tian[2,5], L-Q Zhu[2,5] and Y Lu[1,2]

The entorhinal cortex (EC) is one of the most vulnerable brain regions that is attacked during the early stage of Alzheimer's disease (AD). Here, we report that the synaptic terminals of pyramidal neurons in the EC layer II ($ECII_{PN}$) directly innervate CA1 parvalbumin (PV) neurons ($CA1_{PV}$) and are selectively degenerated in AD mice, which exhibit amyloid-β plaques similar to those observed in AD patients. A loss of $ECII_{PN}$–$CA1_{PV}$ synapses disables the excitatory and inhibitory balance in the CA1 circuit and impairs spatial learning and memory. Optogenetic activation of $ECII_{PN}$ using a theta burst paradigm rescues $ECII_{PN}$–$CA1_{PV}$ synaptic defects and intercepts the decline in spatial learning and memory. These data reveal a novel mechanism of memory loss in AD mice via the selective degeneration of the $ECII_{PN}$–$CA1_{PV}$ pathway.

Molecular Psychiatry (2018) **23,** 199–210; doi:10.1038/mp.2016.151; published online 27 September 2016

INTRODUCTION

The deposition of senile plaques, which primarily consist of amyloid-β peptide, is a major pathological hallmark of Alzheimer's disease (AD) and has long been considered to be associated with a progressive loss of central neurons in certain regions of the brain.[1–3] However, recent studies have shown that spatial learning and memory impairment, an early clinical sign of AD, is caused by synaptic dysfunction rather than neuronal loss, as evidenced in both human patients and transgenic mutant mice.[4–6] The post-mortem hippocampi of AD patients show substantial decreases in synaptic density compared with age-matched controls. In Tg2576-APPswe mice (AD mice) that carry a transgene coding for the 695-amino acid isoform of the human Alzheimer β-amyloid precursor protein with the Swedish mutation and that exhibit plaque pathologies similar to those in AD patients, synaptic strength in the hippocampus exhibits an age-dependent decay preceding the presence of senile plaques.[7–10] These data suggest that early synaptic defects are correlated with the onset of behavioral impairments; however, the direct contribution of these defects requires further study.

Excitatory pyramidal neurons in the entorhinal cortex (EC, EC_{PN}) that primarily target the hippocampus are the most vulnerable brain cells attacked in the early stage of AD.[11–13] Previous studies showed that EC_{PN} in layer II ($ECII_{PN}$) and layer III ($ECIII_{PN}$) regions innervate CA1 pyramidal neurons ($CA1_{PN}$) for spatial memory.[14–17] A surgical lesion of EC_{PN} inputs to $CA1_{PN}$ impairs spatial representations.[18,19] A recent report demonstrated that $ECII_{PN}$ axon terminals form excitatory synapses directly with γ-aminobutyric acid interneurons in the CA1 hippocampus ($CA1_{IN}$), and this direct pathway is an essential circuit for temporal association memory.[20] However, several types of $CA1_{IN}$ are expressed in the adult brain, and the types of $CA1_{IN}$ that receive excitatory inputs from $ECII_{PN}$ remain unknown.

Here, we discovered that $ECII_{PN}$ directly innervate the parvalbumin (PV) subtype of $CA1_{IN}$ ($CA1_{PV}$). We showed that this $ECII_{PN}$–$CA1_{PV}$ pathway is selectively degenerated in an early stage of AD. Furthermore, optogenetic activation of $ECII_{PN}$–$CA1_{PV}$ synapses with a theta burst stimulation (TBS) paradigm effectively intercepted the progression of $ECII_{PN}$–$CA1_{PV}$ synaptic decays and improved spatial learning and memory in AD mice.

MATERIALS AND METHODS

Animals

All mice used in this study were bred and reared in the same conditions in accordance with institutional guidelines and the Animal Care and Use Committee (Huazhong University of Science and Technology, Wuhan, China) of the university's animal core facility. The mice were housed in groups of three to five per cage under a 12-h light–dark cycle, with lights on at 0800 h, at consistent ambient temperature (21 ± 1 °C) and humidity (50 ± 5%). The AD (Tg2576-APPswe) mice used in this study were identified as homozygous. In the present study, male mice were used to avoid behavioral variabilities between genders. All the experiments and analyses were performed blind to genotype or treatment.

Generation of the mutant mice

To determine a direct synaptic connection between $ECII_{PN}$ and $CA1_{PV}$, we created a mutant line of mice with a loxP-flanked STOP sequence followed by the avian viral receptor TVA and rabies G and mCherry (TVA/$G^{loxP/loxP}$ mice). The Rosa-CAG-Flag-TVA/G-WPRE targeting vector was designed with a CMV-IE enhancer/chicken β-actin/rabbit β-globin hybrid promoter (CAG), an FRT site, a loxP-flanked STOP cassette, a Flag-TVA/G sequence, WPRE (a woodchuck hepatitis virus posttranscriptional regulatory element; to enhance the mRNA transcript stability), a poly-A signal and an attB/att-

[1]Department of Physiology, School of Basic Medicine and Tongji Medical College, Huazhong University of Science and Technology, Wuhan, China; [2]The Institute for Brain Research, Collaborative Innovation Center for Brain Science, Huazhong University of Science and Technology, Wuhan, China; [3]Department of Neurobiology, Tongji School of Basic Medicine, Huazhong University of Science and Technology, Wuhan, China; [4]Department of Genetics, Tongji School of Basic Medicine, Huazhong University of Science and Technology, Wuhan, China and [5]Department of Pathophysiology, Tongji School of Basic Medicine, Huazhong University of Science and Technology, Wuhan, China. Correspondence: Dr L-Q Zhu or Dr Y Lu, Department of Physiology, School of Basic Medicine and Tongji Medical College, Huazhong University of Science and Technology, Wuhan 430030, China.

E-mail: zhulq@hust.edu.cn or lym@hust.edu.cn

[6]Co-first authors.

Received 23 February 2016; revised 16 May 2016; accepted 13 July 2016; published online 27 September 2016

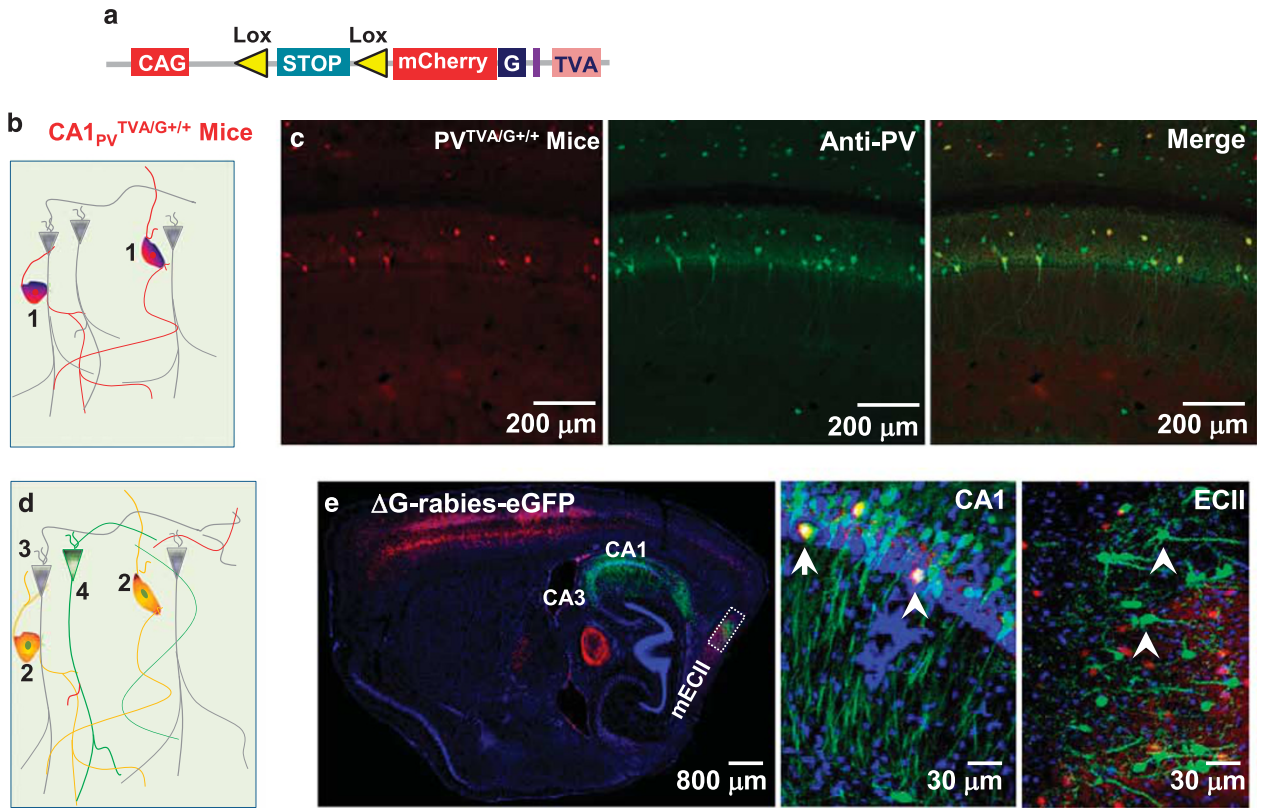

Figure 1. $ECII_{PN}$ directly innervates $CA1_{PV}$. (**a**) The construct used to generate the mutant mice with the expression of TVA, and G and mCherry proteins. (**b** and **c**) An illustration (**b**) and a brain section (**c**) from a $PV^{TVA/G+}$ mouse showing the expression of TVA/G and mCherry proteins in the PV cells that were recognized using an antibody against PV protein. (**d**) Illustration showing the expression of two proteins (TVA and G) in $CA1_{PV}$ (red) necessary for subsequent rabies infection and monosynaptic retrograde spread. The ΔG-rabies-eGFP virus particles infect a TVA/G-expressing $CA1_{PV}$ (cell 2, yellow) and undergo monosynaptic retrograde spread to $CA1_{PN}$ (cell 4, green). (**e**) A merged image of a brain section from $PV^{TVA/G+}$ (red) mice injected with ΔG-rabies-eGFP (green) and stained with DAPI (blue) showing eGFP expression in $CA1_{PN}$ (green), $CA3_{PN}$ and $ECII_{PN}$ (green). High magnifications of the CA1 and ECII regions showing the expression of ΔG-rabies-eGFP in $CA1_{PV}^{TVA/G+}$ cells (yellow, arrow) and monosynaptic retrograde labeling of $CA1_{PN}$ and $ECII_{PN}$ (green, arrowheads). Similar results were observed in each of the five male C57Bl/6 mice at 120 ± 2 days of age ($n = 5$ mice per group). EC, entorhinal cortex; eGFP, enhanced green fluorescence protein; PV, parvalbumin.

flanked PGK-FRT-Neo-poly-A cassette. This entire construct was inserted into the Gt(ROSA)26Sor locus via electroporation in C57BL/6-derived embryonic stem cells. The targeted embryonic stem cells were selected and injected into C57BL/6 blastocysts, and chimeric animals were bred to C57BL/6 mice. When bred to PV-Cre knock-in mutant mice (The Jackson Laboratory, Bar Harbor, ME, USA, Stock No. 008069), in which Cre recombinase was expressed in PV neurons, the mice expressed TVA/G in PV neurons ($PV^{TVA/G+/+}$ mice). A high titer (200 nl of 3×10^9 genomic particles per ml, provided by Dr Fuqiang Xu at the Wuhan Institute of Physics and Mathematics, Chinese Academy of Sciences) of the Enva-ΔG-rabies virus encoding enhanced green fluorescence protein (eGFP) was stereotaxically injected into the CA1 hippocampus of the $PV^{TVA/G+}$ mice, leading to a specific monosynaptic retrograde labeling of the $CA1_{PV}$ presynaptic cells, including $CA1_{PN}$ and $ECII_{PN}$.

To express ChR2-eGFP in the $ECII_{PN}$ of AD mice, we created a mutant strain of mice that had a loxP-flanked STOP sequence followed by the ChR2 (E123A)-eGFP. The Rosa-CAG-Flag-ChR2-eGFP-WPRE targeting vector was designed using a CMV-IE enhancer/chicken β-actin/rabbit β-globin hybrid promoter (CAG), an FRT site, a loxP-flanked STOP cassette, a Flag-eGFP sequence, WPRE (to enhance the mRNA transcript stability), a poly-A signal and an attB/att-flanked PGK-FRT-Neo-poly-A cassette. This entire construct was inserted into the Gt(ROSA)26Sor locus via electroporation in C57BL/6-derived embryonic stem cells. The targeted embryonic stem cells were selected and injected into C57BL/6 blastocysts, and chimeric animals were bred to C57BL/6 mice ($ChR2^{loxP/loxP}$).

We next created rAAV1/2-D28K-Cre virus particles. We designed the rAVE-D28K-Cre vector via the insertion of a Cre recombinase sequence immediately downstream of the calbindin 1 (or calbindin-D28K, D28K) translational STOP codon through *ApaI*/*KpnI*. The rAVE plasmids were co-transfected with the AAV helper1/2 mixers into HEK293 cells to generate the rAAV1/2-D28K-Cre virus particles with a high titer ($> 5 \times 10^{12}$ genomic particles per ml), as described previously.[21,22] The virus particles (1.5 μl) were bilaterally injected into the superficial layer of the EC of $AD/ChR2^{loxP/loxP}$ and $control/ChR2^{loxP/loxP}$ mice, resulting in ChR2-eGFP expression in the $ECII_{PN}$ of the AD or control mice ($AD/ECII_{PN}^{ChR2+}$ and $control/ECII_{PN}^{ChR2+}$ mice, respectively). As shown in Figure 3 and Figures 4b and c, eGFP was expressed in the $CA1_{PV}$ of the $AD/ECII_{PN}^{ChR2+}$ mice due to the injection of 2 μl of a high titer (3×10^{-13} genomic particles per ml) of the rAAV1/2-PV-eGFP virus directly into the CA1 hippocampus of the $AD/ECII_{PN}^{ChR2+}$ mice or $control/ECII_{PN}^{ChR2+}$ mice.

Optogenetic stimulations

The mice were anesthetized with 6% chloral hydrate (0.06 ml per 10 g; intraperitoneally). Four tetrodes of twisted 17 μm HM-L coated platinum–iridium (10% or 20% platinum, #100-167, California Fine Wire, Grover Beach, CA, USA) wire were connected to a microdrive to enable dorsoventral adjustment of the tetrodes after surgery. The tetrodes were directly positioned above the recording site. The microdrive was secured to the skull using jeweler's screws and dental cement. A jeweler's screw fixed to the skull served as a ground electrode. Daily screening for cells and behaviors began according to the experimental procedure. The tetrodes were lowered slowly over several days in steps of 30 μm.

A 200 μm-diameter, unjacketed optical fiber (Ocean Optics) bound to the tetrode-contained silicone tube (166 μm) was bilaterally implanted into the ECII regions (anteroposterior: 4.8, mediolateral: 2.8 and dorsoventral: 3.5–4.0; locations were validated by electrolytic lesions after light stimulation) and secured to the skull using jeweler's screws and dental cement. The animals were used for the experiments 7 days after the

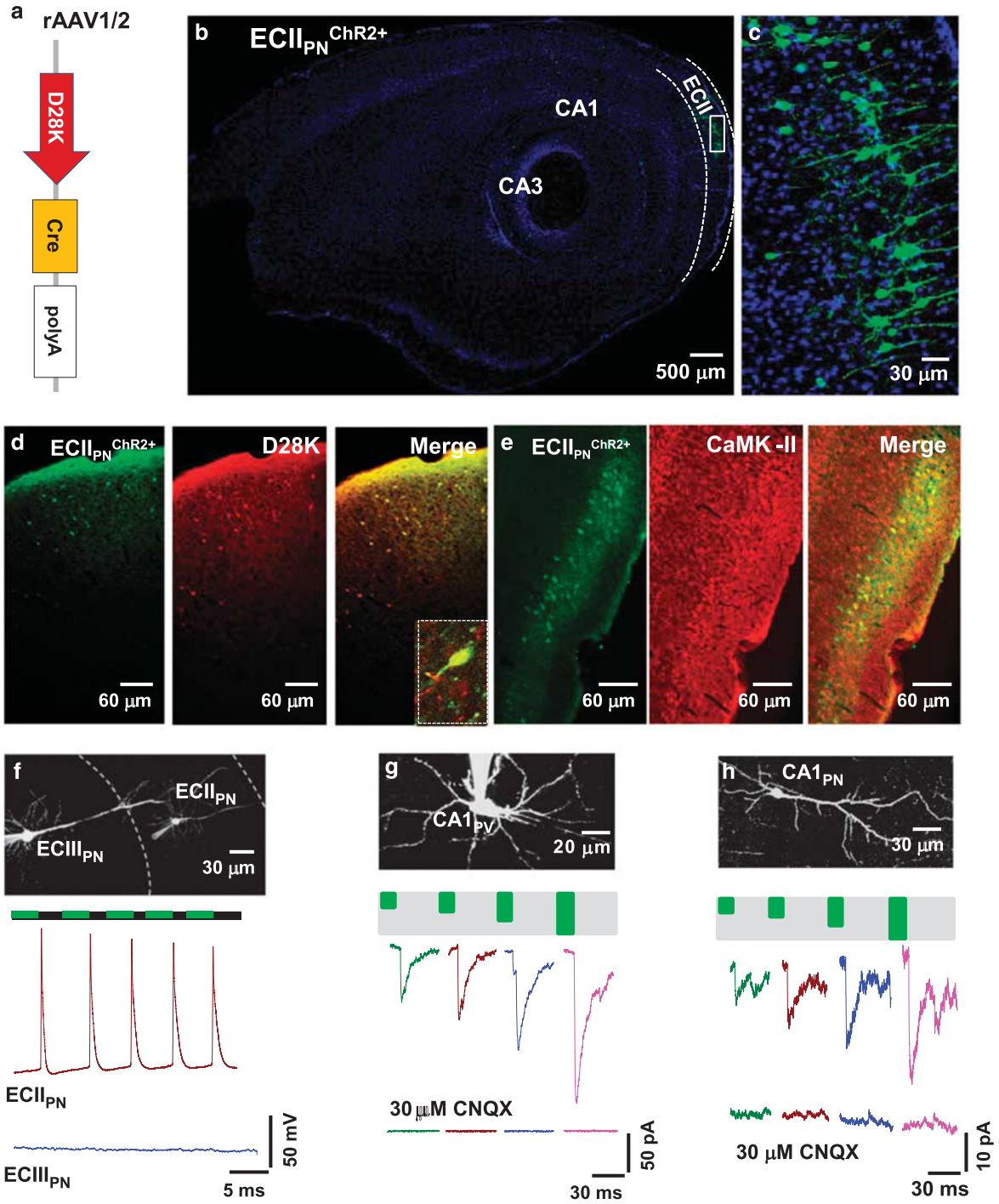

Figure 2. ECII$_{PN}$ functionally targets CA1$_{PV}$ via a direct pathway. (**a**) rAAV1/2 vector for the expression of Cre under control of the D28K promoter. (**b**) A brain section from a ChR2$^{loxP/loxP}$ mouse injected with 1.2 μl of the AAV1/2 virus particles in the ECII region and stained with DAPI. (**c**) High magnification of a selected area showing the ChR2-eGFP expression in ECII$_{PN}$. (**d**) An EC region from a ChR2$^{loxP/loxP}$ mouse injected with the AAV1/2-D28K-Cre virus (green) and stained with an antibody against the D28K protein (red). (**e**) An EC region from a ChR2$^{loxP/loxP}$ mouse injected with the AAV1/2-D28K-Cre virus (green) and stained with an antibody against CaMKIIα protein (red). (**f**) Double whole-cell patch clamp recordings from ECII$_{PN}$ and ECIII$_{PN}$ in a slice from a ECII$_{PN}^{ChR2+}$ mouse. Representative recordings of action potential firings in ECII$_{PN}$, but not in ECIII$_{PN}$, in response to blue laser light illuminations in ECII$_{PN}$. (**g**) Evoked excitatory postsynaptic currents (EPSCs) in CA1$_{PV}$ in response to increased intensities of blue laser light in the absence or presence of 30 μM CNQX in slices from a ECII$_{PN}^{ChR2+}$ mouse. (**h**) Evoked EPSCs in CA1$_{PN}$ in response to increased intensities of blue laser light in the absence or presence of 30 μM CNQX in slices from a ECII$_{PN}^{ChR2+}$ mouse. In (**b**–**h**), similar results were observed in each of the five male C57Bl/6 mice at 120 ± 2 days of age ($n = 5$ mice per group). EC, entorhinal cortex; eGFP, enhanced green fluorescence protein; PV, parvalbumin.

implantation. Light pulses and TBS were generated using a 473 nm laser (DPSS laser, Anilab Software & Instruments, Ningbo, China) controlled via a computer. The laser power was regulated according to the penetration rate of the fiber in the electrode, and the final laser power ranged from 0.1 to 5 mW mm^{-2}.

For TBS treatment, the male AD mice at 120 days of age that had the breeding condition, body weight and behavioral activities, similar to those of the age-matched control mice were randomly selected for the treatment. $ECII_{PN}$ were stimulated using blue light pulses that consisted of 10 trains of stimuli at 10 s intervals, with each train containing bursts of four spikes at 100 Hz and repeated 10 times at 5 Hz, where the duration of each spike was 5 ms using a 473-nm wavelength laser at power densities ranging from 0.1 to 5 mW mm^{-2} using a DPSS laser (Anilab). The mice received bilateral TBS stimulations once per day for 35 consecutive days. The mice were used for the experiments 25 days after the treatment. In this study, TBS treatment was done by the experimenter (XY) who was unaware of the genotypes.

Extracellular single-unit recording

Extracellular single-unit and local field power spectrum, recordings were made from the CA1 neurons (anteroposterior: − 1.7, mediolateral: 1.0 and dorsoventral: 0.5–0.8 target to CA1). The mice were connected to the recording equipment via AC-coupled unity-gain operational amplifiers (Plexon, Dallas, TX, USA). The signals were amplified 4000- to 8000-fold. The spikes and local field potentials were recorded at the same time and isolated using a 250 Hz lowpass filter and a 250 Hz highpass filter of the commercial software OmniPlex (Plexon). In this study, the recordings in Figure 4 were done by the experimenter (TT) who did not know whether the mice were treated with or without TBS treatment.

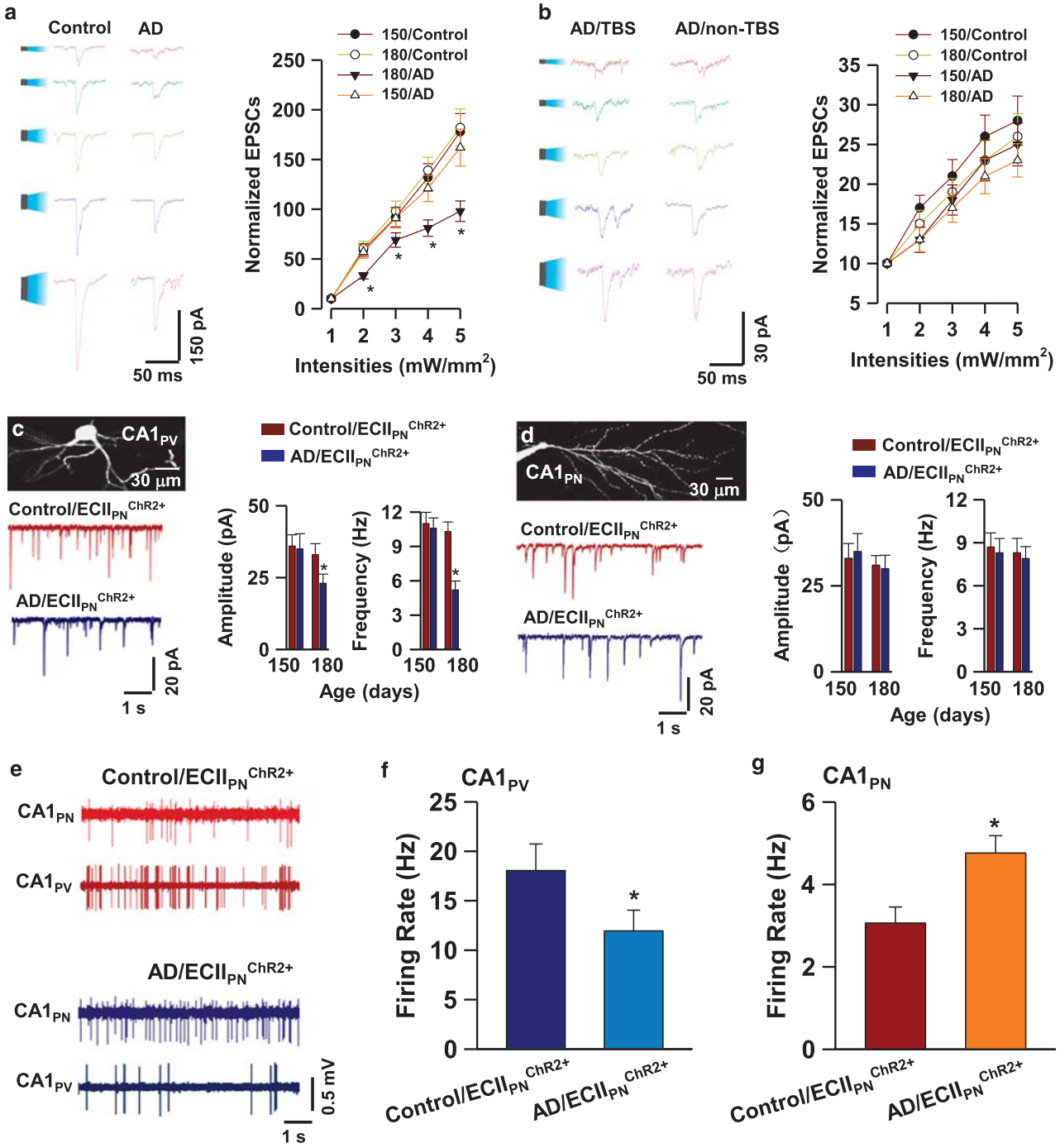

Spike sorting and analysis

Spike sorting was performed offline using graphical cluster-sorting software (Offline Sorter, Plexon). To estimate the quality of the cluster separation, we calculated the isolation distance and the L-ratio using Plexon SDK (www.plexon.com/software-downloads/SDK). Only the units with an L-ratio less than 0.05 and a distance greater than 15 were included.

To isolate and analyze spike units from individual neuronal types, we calculated the valley-to-peak time and the half-width of the spikes. Spikes in $CA1_{PN}$ were identified and distinguished from the $CA1_{IN}$ based on the duration of the negative spike, the firing pattern (complex spikes) and the low-average firing rate. Spikes in the $CA1_{PV}$ were validated via light stimulation of the $CA1_{PV}^{ChR2+/+}$ neurons of $PV^{ChR2+/+}$ mice, which were generated by crossing $ChR2^{loxP/loxP}$ mice with PV-Cre mice. The average firing rate was expressed as the total number of spikes divided by the total length of the recording period.

Local field power spectrum

The local field power spectrum from 0 to 100 Hz was computed before, during and after TBS treatment. For the local field power spectrum trace, a 4–10 Hz bandpass filter was used to separate the theta band and a 30–90 Hz bandpass filter was used to divide the gamma band. For the power spectra analysis, the power spectra were averaged separately before and after TBS treatment. In AD mice, the TBS stimulations of the $ECII_{PN}$ generated theta oscillations in the CA1 neurons. Light stimulation of the $ECII_{PN}$ at 20–30 Hz generated gamma oscillations and, in some cases, enhanced theta oscillation several seconds after the 20–30 Hz stimulation.

Place field analysis

For place cell recordings, the optical fiber was cut off and a custom-made tetrode was implanted via a pre-drilled hole (above the CA1) and secured to the skull using dental cement. After 3–4 days of recovery, daily screening for cells and spontaneous behaviors were initiated in an open field. A tracker system (CinePlex, Plexon) was used to record the position of a red LED attached to the head stage. The place field analysis was performed using the commercial software Neuroexplorer (Plexon). the spike density and position (animal coordinates) were sampled synchronously and a rate map was calculated for pixels of 5×5 cm that were visited by the mice. In all the groups, all pyramidal units that had average firing rates above 0.25 Hz were included in the analysis. We also defined the 'place field' as a contiguous region of at least 8 pixels (200 cm^2) in which the firing rate exceeded 20% of the peak rate. The 'place field size' was considered the largest detected field size. The 'information density' was estimated as how much information a single spike conveys and was defined according to a previously described formula.[18]

Electrolytic lesions and immunohistochemistry

Electrolytic lesions were induced after the *in vivo* recording or stimulation treatment via the pre-moded electrode above the skull or a multi-electrode connected to an external electrical source. Electrolytic lesions were induced using a constant direct current of 1.0 mA for 20 s. The mice were killed via an intraperitoneal injection of an overdose of chloral hydrate and were then transcardially perfused with 100 ml saline (0.9% w/v NaCl) followed by 4% paraformaldehyde. The brains were removed and post-fixed in 4% paraformaldehyde. Thirty-micrometer sagittal or horizontal sections were cut (Leica Microsystems, Wetzlar, Germany). Immunohistochemistry was performed on free-floating brain sections, as described previously, using anti-calbindin-D-28 K (1:1000, AB1778, Millipore Sigma, Merck, Darmstadt, Germany) or anti-CaMKII (1:2000, AB3865, Millipore Sigma), anti-DAPI (1:500, AB156693, Abcam, Cambridge, UK), anti-reelin (1:500, AB138370, Abcam), β-amyloid or 17–24 (4G8) monoclonal antibody (1:1000, NE1002, Millipore Sigma).

Open-field tests and rotarod test

Locomotor activity was measured within clear boxes measuring 100 cm × 100 cm and outfitted with photo-beam detectors for monitoring horizontal and vertical activity, as described previously.[21] The data were collected via a PC and were analyzed using the MED Associates' Activity Monitor Data Analysis software. The mice were placed in a corner of the open-field apparatus and allowed to move freely. The variables recorded included resting time (s), ambulatory time (s), vertical/rearing time (s), jump time (s), stereotypic time (s) and average velocity (cm s^{-1}). The mice were not exposed to the chamber before testing. The data were recorded for each individual animal during 30 min intervals. For the rotarod test, the mice were subjected to a 1 -week learning period, after which they were able to perform on an accelerating rotarod. The test was then performed twice per week until the mice were unable to remain on the rotating bar for more than 10 s on three consecutive attempts, which was defined as rotarod failure.

Morris water maze

A pool 1.5 m in diameter filled with water was made opaque with a white, nontoxic ink maintained at 25 °C. After the final TBS stimulation, the animals were brought to the behavior room (where they were housed for the duration of the training), handled for 1–2 days, and trained, as described previously.[21–24] The full protocol lasted 7 days. The first training day consisted of a probe trial followed by a 'visible platform' trial, in which the platform was indicated by a red flag. Next, the mice underwent their first 'hidden platform' learning trial, during which they were allowed to rest on the platform for 30 s before being released from one of the pool's starting points (north, south, east or west). The animals were allowed 60 s to find the platform and allowed to remain on the platform for 30 s; if animals did not find the platform within 60 s, they were removed from the water and placed on the platform for 30 s. During days 1 through 6, four trials were performed, corresponding to four different randomized release points. Therefore, the total training took 6 days followed by the 24 h probe on the seventh day. In this study, behavioral tests were done by the experimenter (CY) who was unaware of the genotypes and the treatments.

Figure 3. Selective degeneration of the EC_{PN}–CA1pv pathway in AD mice. (**a**) The normalized mean amplitudes of the excitatory postsynaptic currents (EPSCs) of $CA1_{PV}$ are reduced in AD mice. The representative traces show EPSCs in $CA1_{PV}$ evoked by blue laser light illuminations of $ECII_{PN}$ at intensities of 1 to 5 mW mm^{-2} in the slices from the AD/$ECII_{PN}^{ChR2+}$ and control/$ECII_{PN}^{ChR2+}$ mice at 150 and 180 days of age, respectively. The mean amplitudes of the EPSCs are normalized to those evoked at an intensity of 1.0 mW mm^{-2} (defined as 10) and plotted against the light intensity. Data are reported as the mean ± s.e.m. ($n = 36$ cells per nine mice per group, $^*P < 0.001$, *t*-test). (**b**) The mean amplitudes of the evoked EPSCs in $CA1_{PN}$ are normal in the AD mice. Representative traces show the EPSCs of $CA1_{PN}$ evoked by blue laser light illuminations of $ECII_{PN}$ at the intensities of 1 to 5 mW mm^{-2} in slices from the AD/$ECII_{PN}^{ChR2+}$ and the control/$ECII_{PN}^{ChR2+}$ mice at 150 and 180 days of age, respectively. The mean amplitudes of the EPSCs are normalized to those evoked at an intensity of 1.0 mW mm^{-2} (defined as 10) and plotted against the light intensity. Data are reported as the mean ± s.e.m. ($n = 27$ cells per nine mice per group). (**c**) The mean amplitudes and frequencies of the miniature EPSCs are reduced in the $CA1_{PV}$ of AD mice. A representative $CA1_{PV}$ (top left) that was filled with Alexa594 via a recording electrode and the miniature EPSCs (bottom left) of $CA1_{PV}$ in slices from AD/$ECII_{PN}^{ChR2+}$ and control/$ECII_{PN}^{ChR2+}$ mice. The mean amplitudes and frequencies of the events are summarized in bar graphs. Data are reported as the mean ± s.e.m. ($n = 12$ recordings per three mice per group, $^*P < 0.001$, *t*-test). (**d**) The mean amplitudes and frequencies of the miniature EPSCs are normal from the $CA1_{PN}$ of the AD mice. A representative $CA1_{PN}$ (top left) that was filled with Alexa594 via a recording electrode and the miniature EPSCs (bottom left) recorded from the $CA1_{PN}$ in slices from AD/$ECII_{PN}^{Ch\ R2+}$ and control/$ECII_{PN}^{ChR2+}$ mice. The mean amplitudes and frequencies of the events are summarized in bar graphs. Data are reported as the mean ± s.e.m. ($n = 12$ recordings per three mice per group). (**e**–**g**) Firings decrease in the $CA1_{PV}$ and increase in the $CA1_{PN}$ of AD mice. Representative recordings (**e**) and averaged frequencies (**f** and **i**) of action potential firings in the $CA1_{PV}$ (**f**) and the $CA1_{PN}$ (**g**) of the AD/$ECII_{PN}^{ChR2+}$ mice at 180 days of age and the age-matched nontransgenic control/$ECII_{PN}^{ChR2+}$ mice. AD, Alzhemer's disease; EC, entorhinal cortex; PV, parvalbumin.

Electrophysiology *in vitro*

Hippocampal slices (300 μm) were prepared as described previously.[21–24] The slices were transferred to a holding chamber containing artificial cerebrospinal fluid (in mM: 124 NaCl, 3 KCl, 26 $NaHCO_3$, 1.2 $MgCl_2{\cdot}6H_2O$, 1.25 $NaH_2PO_4{\cdot}2H_2O$, 10 $C_6H_{12}O_6$ and 2 $CaCl_2$ at pH 7.4, 305 mOsm). The slices were allowed to recover at 31.5 °C for 30 min and then at room temperature for 1 h. Acute slices were transferred to a recording chamber continuously superfused with oxygenated artificial cerebrospinal fluid (2 ml min^{-1}) and maintained at room temperature. For whole-cell patch clamp recordings from the CA1 pyramidal cells, hippocampal slices were visualized via IR-DIC using an Axioskop 2FS equipped with Hamamatsu C2400-07E optics (Hamamatsu City, Japan). When stable whole-cell recordings were achieved with good access resistance (~20 MΩ), basic electrophysiological properties were recorded. The miniature excitatory postsynaptic currents (EPSCs) were recorded using an internal solution containing (in mM) 140 potassium gluconate, 10 HEPES, 0.2 EGTA, 2 NaCl, 2 MgATP and 0.3 NaGTP, and an external solution containing 10 μM bicuculline, 1 μM TTX or using 10 μM CNQX and 50 μM APV (miniature inhibitory postsynaptic currents or spontaneous inhibitory PSCs without TTX). The data were collected at 10 kHz and filtered with a lowpass filter at 2 kHz. Miniature events were analyzed in Clampfit 10.2 software (Molecular Devices, Sunnyvale, CA, USA) using template matching and a threshold of 5 pA.

For *in vitro* optogenetic stimulation, a 405 nm laser was used to activate the ChR2-positive neuron. The evoked EPSCs were recorded from slices in an external solution containing 10 μM bicuculline (Tocris, Bristol, UK) or containing 30 μM CNQX (Tocris) and 50 μM APV (Tocris) for evoked inhibitory postsynaptic currents recordings. Light stimulation (10–30% laser, 5–10 ms) was performed 100 μm forward the recording of $CA1_{PN}$ and

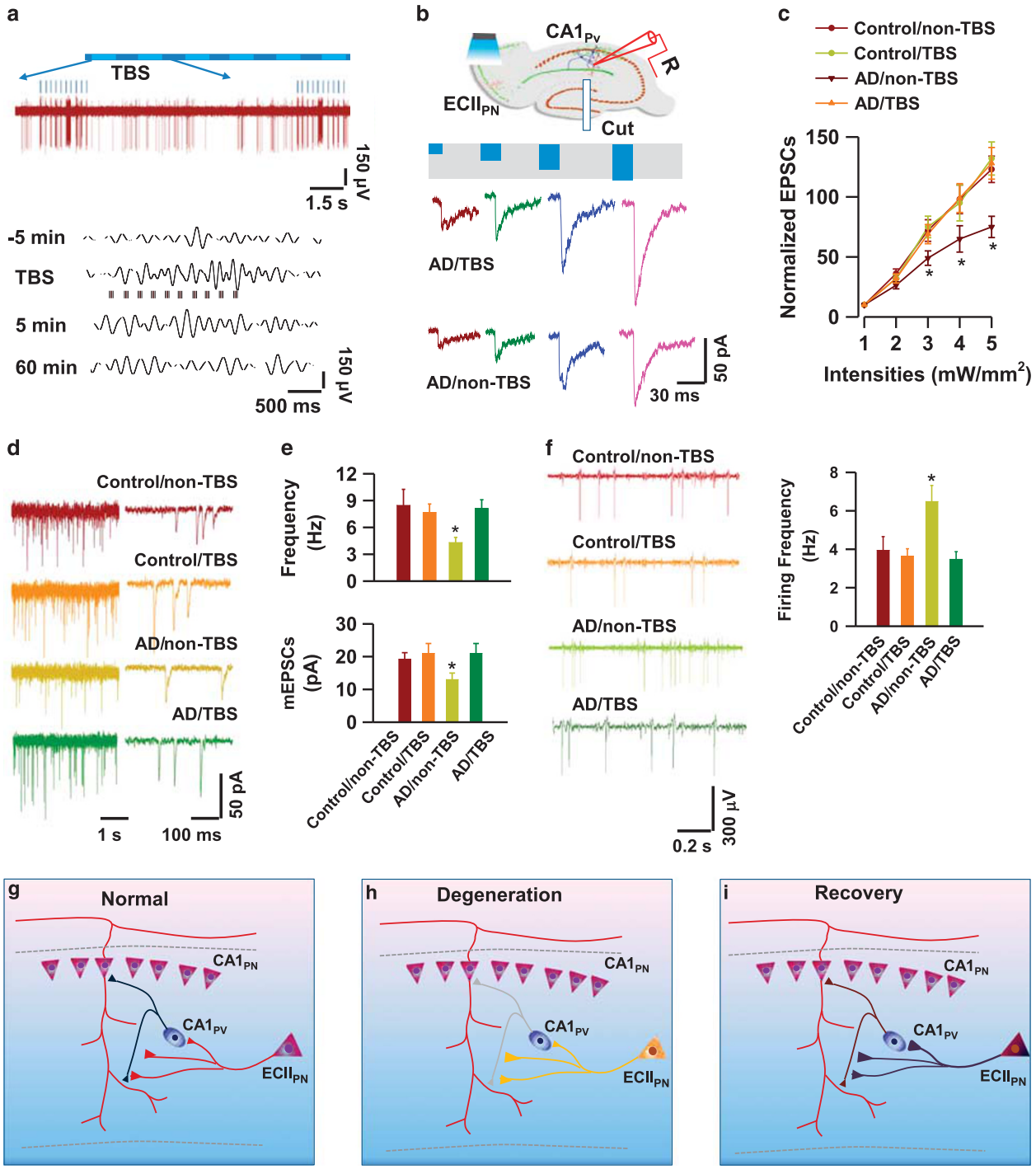

$CA1_{PV}$. In this study, the recordings were done by the experimenter (XY) who was unaware of the genotypes and the treatments.

Data analysis

All variance values in the text and figure legends are represented as the mean ± s.e.m. Parametric tests including unpaired two-tailed Student's *t*-tests and two-way analysis of variance were used where assumptions of normality and equal variance (F test) were met. Significance was accepted for $P < 0.01$. Power calculations were performed using G*power software v3.1.9.2 (IDRE Research Technology Group, Los Angeles, CA, USA). Group sizes were estimated on the basis of the recent studies[21–23] and they were made to provide at least 80% power with the following parameters: probability of type I error (α) = 0.05, a conservative effect size of 0.25, three to eight treatment groups with multiple measurements obtained per replicate.

RESULTS

$ECII_{PN}$ directly innervate $CA1_{PV}$

To determine direct synaptic connections from $ECII_{PN}$ to $CA1_{PV}$, we created a mutant line of mice that expressed the avian viral receptor TVA and rabies G fused to mCherry ($TVA/G^{loxP/loxP}$ mice, Figure 1a). When crossed with the PV-Cre mice, TVA/G protein was expressed specifically in the PV cells in the brain ($PV^{TVA/G+/+}$ mice, Figures 1b and c). Next, we stereotaxically injected a high titer (200 nl of 3×10^9 genomic particles per ml) of the Enva-ΔG-rabies virus encoding eGFP into the CA1 hippocampus of the $PV^{TVA/G+/+}$ mice (Figure 1d). Seven days after the injection, the brain sections were processed. A bright fluorescence signal (eGFP) was detected in the $mCherry^+$ $CA1_{PV}$ ($eGFP^+/mCherry^+$) and their direct presynaptic inputs, such as locally connected $CA1_{PN}$ and $CA3_{PN}$ ($eGFP^+$, Figure 1e), showing that the ΔG-rabies virus can infect and spread in a retrograde fashion across monosynaptic connections. In addition, we observed ΔG-rabies-eGFP expression in a group of $ECII_{PN}$ ($ECII_{PN}^{eGFP+}$, Figure 1e). ΔG-rabies-eGFP expression was undetectable in $ECIII_{PN}$ and $mCherry^+$ PV cells in the mEC region. These results demonstrate that $CA1_{PV}$ receive synaptic inputs directly from $ECII_{PN}$. Recent reports have revealed two major groups of excitatory ECII neurons—ocean cells and island cells—which differ in their molecular markers, anatomical features and projection targets.[20,25] Our studies using immunostaining showed that $ECII_{PN}$ that directly innervate the $CA1_{PV}$ were co-labeled with antibodies against Wfs1 and D28K proteins, but not reelin, and hence, these cells made up a group of island cells (Supplementary Figure S1).

To determine the functional properties of the $ECII_{PN}$–$CA1_{PV}$ pathway, we engineered $ECII_{PN}$ expressing channelrhodopsin-2-E123A (ChR2), a modified version of a light-gated cation channel.[26] Specifically, we created a conditional line of mutant mice with the expression of a double-floxed inverted open reading frame of ChR2-eGFP ($ChR2^{loxP/loxP}$ mice). We also constructed the type 1/2 recombinant adeno-associated (rAAV1-/2)-D28K-Cre virus vector, in which Cre recombinase was expressed under control of the D28K promoter (Figure 2a). A high titer of the virus particles was injected directly into the ECII of $ChR2^{loxP/loxP}$ mice. Thirty days after the injection, the brain sections were imaged (Figures 2b and c) and stained with an antibody against D28K (Figure 2d), which was expressed in the $ECII_{PN}$.[20,27–29] The $ChR2^+$ cells were reactive to an antibody against CaMK-IIα (Figure 2e). Together, the findings showed that AAV1/2-induced ChR2-eGFP expression was primarily located in excitatory $ECII_{PN}$ ($ECII_{PN}^{ChR2+}$ mice). A specific expression of functional ChR2 channels in $ECII_{PN}$ of $ECII_{PN}^{ChR2+}$ mice was observed in whole-cell patch clamp recordings, which revealed blue laser light illuminations of $ECII_{PN}$-evoked action potentials in $ECII_{PN}$, but not in $ECIII_{PN}$ (Figure 2f), and reliable EPSCs in $CA1_{PV}$ (the maximal amplitude of 172 ± 13 pA, mean ± s.e.m., $n = 28$ recordings per five mice; Figure 2g). The mean latencies were 1.98 ± 0.26 ms ($n = 28$ recordings per five mice, mean ± s.e.m.), which is in line with monosynaptic transmission. Under the same intensities of light illuminations of $ECII_{PN}$, only small amplitudes of the EPSCs were evoked in $CA1_{PN}$ (the maximal amplitude of 27.3 ± 3.1 pA, mean ± s.e.m., $n = 28$ recordings per five mice; Figure 2h). Together, these data demonstrate that $ECII_{PN}$ primarily innervates $CA1_{PV}$ via a direct pathway.

Degeneration of the $ECII_{PN}$–$CA1_{PV}$ pathway in AD mice

Having determined a direct synaptic pathway of $ECII_{PN}$ to $CA1_{PV}$, we next examined whether this pathway is affected in AD. We prepared hippocampal sections from AD mice (homozygous Tg2576-APPswe mice with C57BL/6 genetic background), which exhibited amyloid-β plaque pathologies similar to those observed in AD patients (Supplementary Figure S2). First, we determined the functions of the $ECII_{PN}$–$CA1_{PV}$ pathway in AD mice. We crossed the $ECII_{PN}^{ChR2+}$ mice with AD ($AD/ECII_{PN}^{ChR2+}$) or control ($control/ECII_{PN}^{ChR2+}$) mice. Whole-cell patch clamp recordings from both $CA1_{PV}$ (Figure 3a) and $CA1_{PN}$ (Figure 3b) were performed on slices prepared from the $AD/ECII_{PN}^{ChR2+}$ mice at 150 ± 5 days and 180 ± 5 days of ages and from respective age-matched controls. The $AD/ECII_{PN}^{ChR2+}$ mice at 180 ± 5 days were used for the experiments because they show memory loss at that period of time. EPSCs at a holding potential of − 70 mV were evoked by the delivery of blue laser lights directly to the $ECII_{PN}$. The average

Figure 4. Optogenetic intervention of $ECII_{PN}$-$CA1_{PV}$ synaptic decays. (**a**) Representative recordings of action potential firings (top, purple trace) in the $CA1_{PV}$ and theta waves (bottom, black) in response to TBS treatment in the CA1 hippocampus of male $AD/ECII_{PN}^{ChR2+}$ mice at 120 days of age 5 min before (−5 min), during (TBS) and 5 (5 min) or 60 (60 min) minutes after TBS. (**b**) Experimental arrangement (top) of the recordings from the $CA1_{PV}$ and stimulation of the $ECII_{PN}$ in *in vitro* brain slices. Representative excitatory postsynaptic currents (EPSCs; bottom) are the response to the increasing intensities of blue laser light (blue bars) in slices from the $AD/ECII_{PN}^{ChR2+}$ mice with (AD/TBS) or without TBS treatment (AD/non-TBS). (**c**) The mean amplitudes of the EPSCs in the $CA1_{PV}$ of the $control/ECII_{PN}^{ChR2+}$ (control) and $AD/ECII_{PN}^{ChR2+}$ (AD) mice with (TBS) or without TBS (non-TBS) treatment are plotted against the light intensity administered to the $ECII_{PN}$. Data are reported as the mean ± s.e.m. ($n = 25$ cells per five mice per group, $F_{(3,96)} = 3.76$, $^*P < 0.001$, two-way analysis of variance (ANOVA)). (**d** and **e**) Representative recordings (**d**) of the miniature EPSCs (mEPSCs) of the $CA1_{PV}$ from the $AD/ECII_{PN}^{ChR2+}$ (AD) and $control/ECII_{PN}^{ChR2+}$ (control) mice with or without TBS treatment. The frequency and the mean amplitudes of the mEPSCs are shown in the bar graphs (**e**). Data are reported as the mean ± s.e.m. ($n = 18$ recordings per six mice per group, $F_{(3,68)} = 4.66$; $P < 0.001$; two-way ANOVA). (**f**) Recovery of excitatory and inhibitory synaptic balance in the CA1 neural circuits of the $AD/ECII_{PN}^{ChR2+}$ mice with TBS treatment. Representative recordings (left) and average frequency of action potential firings of the $CA1_{PN}$ (right) in freely moving $control/ECII_{PN}^{ChR2+}$ and $AD/ECII_{PN}^{ChR2+}$ mice 25 days after TBS treatment. Data are reported as the mean ± s.e.m. ($n = 16$ mice per group, $F_{(3,60)} = 7.11$; $P < 001$, two-way ANOVA; 39 and 44 $CA1_{PN}$ units in AD/TBS and AD/non-TBS, respectively). (**g**–**i**) A working model for optogenetic intervention of synaptic degeneration in AD. Under the physiological conditions (**g**), $ECII_{PN}$ form direct excitatory synapses with $CA1_{PV}$ and balance the excitatory/inhibitory synaptic transmission in CA1 circuits. During the disease progression of AD (**h**), $ECII_{PN}$–$CA1_{PV}$ synapses are degenerated. This degeneration disables the excitatory and inhibitory balance as a consequence of a loss of inhibitory inputs from $CA1_{PV}$ to $CA1_{PN}$. Optogenetic TBS stimulation (**i**) effectively intervenes in the degeneration of $ECII_{PN}$–$CA1_{PV}$ synapses and restores the excitatory and inhibitory synaptic balance in the AD mice. AD, Alzhemer's disease; EC, entorhinal cortex; PV, parvalbumin; TBS, theta burst stimulation.

peak amplitude of the EPSCs (evoked at an intensity of 5 mW mm^{-2}) was comparable between the control/ECII$_{PN}^{ChR2+}$ mice and the AD/ECII$_{PN}^{ChR2+}$ mice at 150 days of age (178 ± 19 pA versus 171 ± 16 pA; mean ± s.e.m., $n = 36$ cells per nine mice per group; $P > 0.5$, *t*-tests; Figure 3a), but it decreased significantly in the the AD/ECII$_{PN}^{ChR2+}$ mice at 180 days of age, compared with age-matched control/ECII$_{PN}^{ChR2+}$ mice (83 ± 11 pA versus 167 ± 17 pA; mean ± s.e.m., $n = 36$ cells per nine mice per group; $^*P < 0.001$, *t*-tests Figure 3a). The averaged peak amplitude of the evoked EPSCs in CA1$_{PN}$ was identical between the control/ECII$_{PN}^{ChR2+}$ mice and the AD/ECII$_{PN}^{ChR2+}$ mice even when they were at 180 days of age (23.7 ± 2.2 pA versus 25.2 ± 2.3 pA; mean ± s.e.m., $n = 36$ cells per nine mice per group; $P > 0.5$, *t*-tests; Figure 3b). Consistent with a reduction in the evoked EPSCs, both the amplitude and the frequency of the miniature EPSCs in CA1$_{PV}$ of AD/ECII$_{PN}^{ChR2+}$ mice at 180 days of age decreased significantly compared with the age-matched control/ECII$_{PN}^{ChR2+}$ mice (Figure 3c). In contrast to CA1$_{PV}$, neither the mean amplitude nor frequency of the excitatory events in CA1$_{PN}$ were altered in the AD/ECII$_{PN}^{ChR2+}$ mice (Figure 3d). Together, the findings show that the ECII$_{PN}$–CA1$_{PV}$ pathway is selectively degenerated in the AD mice.

Action potential firings decrease in CA1$_{PV}$ and increase in CA1$_{PN}$ of AD mice

A reduction in ECII$_{PN}$ excitatory inputs to CA1$_{PV}$ that primarily target the dendrites of CA1$_{PN}$ would disrupt the excitatory and inhibitory balance of CA1 neural circuits. To test this possibility, we monitored the activity of CA1 cells in freely moving mice by

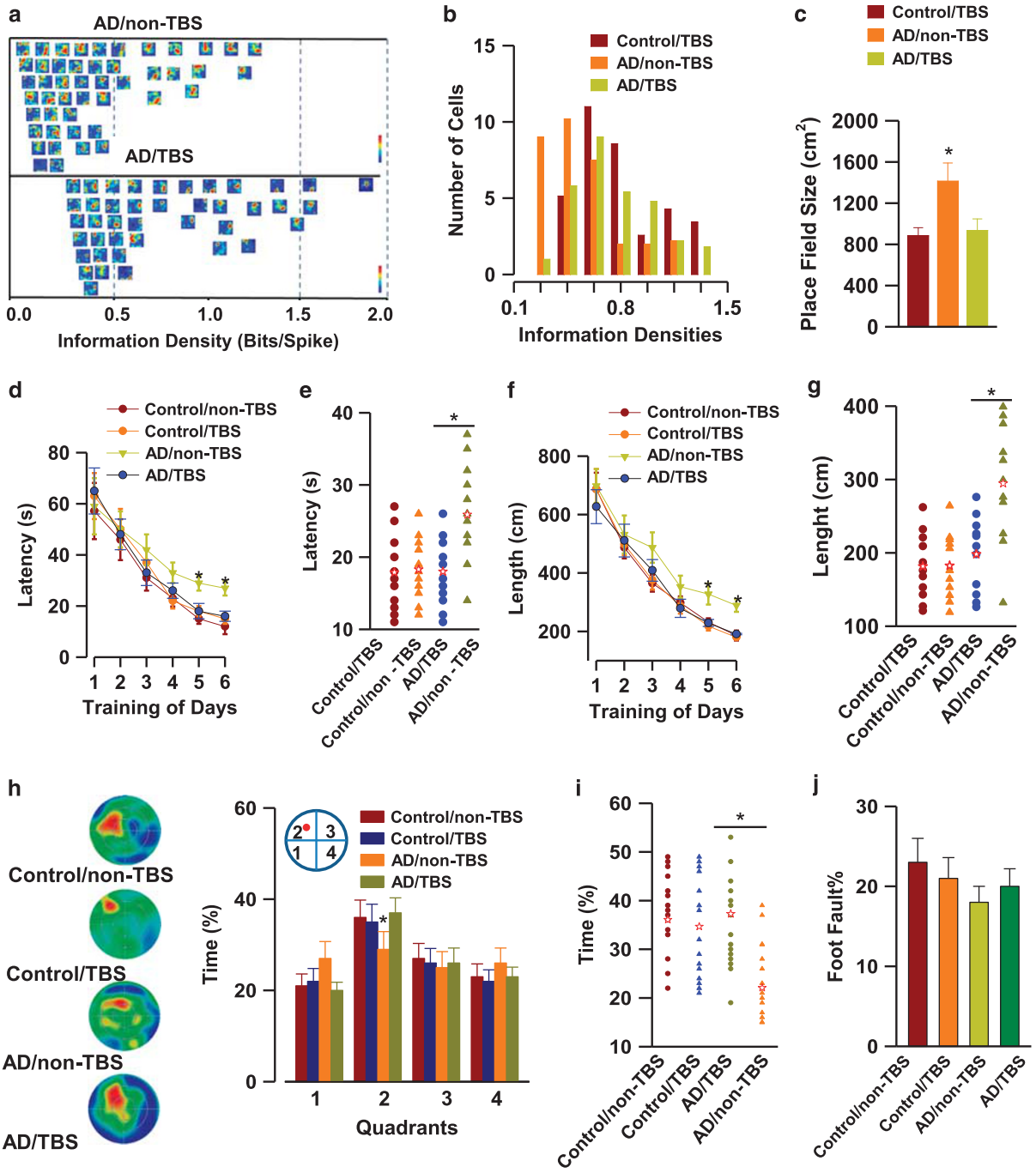

extracellular single-unit recordings. Spike units in $CA1_{PN}$ and in putative CA1 inhibitory interneurons ($CA1_{IN}$) were classified on the basis of their action potential properties by Matlab, and the $CA1_{PV}$ units were isolated via optogenetics (Supplementary Figures S3a–f). Specifically, we generated transgenic mice ($CA1_{PV}^{ChR2+/+}$ mice) expressing ChR2-eGFP in PV neurons by crossing the $ChR2^{loxP/loxP}$ mice with the male PV-Cre mice at 120 ± 2 days of age (Supplementary Figure S3c). Mice at 180 ± 5 days of age were used for the experiments because, during that period of time, synaptic deficits are closely associated with memory loss in AD mice. Due to optogenetic manipulations of $CA1_{PV}$, we found that a brief illumination (50 ms pulse) with blue laser lights reliably and repeatedly induced action potential firings in $CA1_{PV}$ (Supplementary Figure S3d). The sustained illuminations (500 ms pulse) of $CA1_{PV}$ (Supplementary Figure S3f) completely eliminated action potential firings in the neighboring $CA1_{PN}$ in the $PV^{ChR2+/+}$ mice (Supplementary Figure S3f).

Following the identification of action firings in $CA1_{PV}$, we evaluated the excitatory and inhibitory synaptic balance in CA1 circuits in freely moving AD mice. We found that the firing frequency was reduced in the $CA1_{PV}$ of AD/$ECII_{PN}^{ChR2+}$ mice at 180 ± 5 days of age compared with age-matched controls (18.7 ± 2.1 versus 11.3 ± 1.3; mean ± s.e.m., $n = 34$ units per nine mice per group, $P < 001$; *t*-test, Figures 3e and f). This reduction in action potential firings in $CA1_{PV}$ decreased the release of inhibitory γ-aminobutyric acid transmitter from the $CA1_{PV}$ to the $CA1_{PN}$ (Supplementary Figure S4) and increased the firing frequency in the $CA1_{PN}$ from AD mice (3.6 ± 0.38 versus 4.8 ± 0.52; mean ± s.e.m., $n = 41$ units per nine mice per group, $P < 001$; *t*-test, Figure 3g). Together, the data demonstrate that the selective degeneration of the $ECII_{PN}$–$CA1_{PV}$ pathway disables the excitatory and inhibitory synaptic balance in the $CA1_{PN}$ microcircuits and, in turn, enhances $CA1_{PN}$ firing probability in the AD mice. This finding is consistent with the previous studies showing that neuronal activity in the hippocampus is dramatically increased in an early stage of AD.[30,31]

Impairments of spatial learning and memory in AD mice

The failure of the excitatory and inhibitory synaptic balance in CA1 neural circuits might impair spatial learning and memory.[30,31] We thus examined the behavioral performance of AD mice paired with control mice in the Morris water maze. Although the capability for spatial information acquisition was highly variable from mouse to mouse (Supplementary Figures S5a–e), on average, the AD/$ECII_{PN}^{ChR2+}$ mice at 180 ± 5 days of age spent more time searching for a hidden platform in the maze during the training sessions and less time in a targeting quadrant during the probe trials than the age-matched control mice (Supplementary Figures S5f and g). We also analyzed the performance of AD/$ECII_{PN}^{ChR2+}$ mice in the open field. We demonstrated that the AD mice at 180 ± 5 days of age exhibit motor activities similar to those of their age-matched controls (Supplementary Figure S6), indicating that motor activity was normal in early-stage AD in AD/$ECII_{PN}^{ChR2+}$ mice. These data are consistent with most previous reports that spatial learning and memory based on Morris water maze tests are impaired in AD/$ECII_{PN}^{ChR2+}$ mice beginning at 180 days of age.[32–34]

To further determine the specific deficits of spatial learning and memory in AD mice, we carried out place cell recordings and monitored $CA1_{PN}$ firing during spontaneous walking in an open field. Place-specific firing in the $CA1_{PN}$ can reflect spatial retrieval, as determined by path integration-based spatial representations in the EC grid-cell network,[35–37] possibly via a direct EC–$CA1_{PN}$ pathway.[18,19,38] Here, we found that firing maps of $CA1_{PN}$ were generally focused in the control mice, whereas in AD mice at 180 ± 5 days of age, the firings became dispersed (Supplementary Figures S5h and i). Thus, spatial representations are impaired in the AD mice.

Rescue of $ECII_{PN}$–$CA1_{PV}$ synaptic decay in AD mice

Deep brain stimulation (DBS) has shown promise as a therapeutic intervention for some neurological disorders.[39] For example, DBS can mitigate symptoms in AD,[40] Parkinson's disease,[41] epilepsy[42] and depression.[43] These stimulations can induce beneficial effects in the brain. We thus determined whether the optogenetic stimulation of $ECII_{PN}$ in an early stage of AD could rescue $ECII_{PN}$–$CA1_{PV}$ synaptic loss. We tested two types of light illumination of the $ECII_{PN}$ of AD/$ECII_{PN}^{ChR2+}$ mice: 30 Hz blue light pulses and TBS. We found that 30 Hz light stimulations of $ECII_{PN}$ induced gamma oscillations (Supplementary Figure S7a), whereas TBS induced theta oscillations in the CA1 networks of freely moving AD/$ECII_{PN}^{ChR2+}$ mice (Figure 4a and Supplementary Figure S7b).

It was previously reported that hippocampal theta oscillations might encode an animal's position during spatial navigation.[44] Thus, we applied a TBS paradigm in AD/$ECII_{PN}^{ChR2+}$ mice beginning at 120 ± 2 days of age. We used four groups of mice: AD/$ECII^{ChR2+}$ and control/$ECII^{ChR2+}$ mice treated with or without the TBS paradigm. TBS was delivered using 0.2 mm optic fibers bilaterally located in the ECII regions (Supplementary Figure S7c) once per day for 35 consecutive days. Twenty-five days after the final illumination, the theta oscillations were enhanced, whereas gamma oscillations were unchanged, in the AD/$ECII_{PN}^{ChR2+}$ mice

Figure 5. Optogenetic intervention in spatial learning and memory decays. (**a**) Representative rate maps (one map per cell) for $CA1_{PN}$ in the AD/$ECII_{PN}^{ChR2+}$ (AD) and control/$ECII_{PN}^{ChR2+}$ (control) mice with (TBS) or without (non-TBS) TBS treatment. The rate maps are positioned along the *x* axis according to their information density. Dark red corresponds to the maximum firing rate, and dark blue corresponds to no firing (45 units in the control/TBS group, 47 units in the AD/non-TBS group and 41 units in the AD/TBS group). (**b**) An increase in information density in the AD/$ECII_{PN}^{ChR2+}$ (AD) mice following 35 days of TBS treatment. Data are reported as the mean ± s.e.m.. (**c**) A recovery in place field size in the AD/$ECII_{PN}^{ChR2+}$ (AD) and control/$ECII_{PN}^{ChR2+}$ (control) mice following 35 days of TBS treatment (AD/TBS). Data are reported as the mean ± s.e.m. ($n = 15$ mice per group, $F_{(2,42)} = 5.91$; $P < 0.001$; two-way analysis of variance (ANOVA)). (**d**) The average latency to reach a hidden platform is plotted against the blocks of trials. Data are reported as the mean ± s.e.m. ($n = 11$ mice per group, $F_{(3,41)} = 2.26$; $P < 0.001$; two-way ANOVA). (**e**) A plot of the latency for individual animals to reach a hidden platform during the training tests on day 6 ($n = 11$ mice per group, $P = 0.001$; *t*-test). (**f**) The average swim length to reach a hidden platform is plotted against the blocks of trials. Data are reported as the mean ± s.e.m. ($n = 11$ mice per group, $F_{(3,41)} = 2.33$; $P < 0.001$; two-way ANOVA). (**g**) A plot of the swim length for individual animals to reach a hidden platform during training tests on day 6 ($n = 11$ mice per group, $P < 0.001$; *t*-test). (**h**) The average percentage of time spent in search of a hidden platform in each quadrant during the probe trial. Representative hot spots of path tracings are taken from the probe trials on day 8. Data are reported as the mean ± s.e.m. ($n = 11$ mice per group, $F_{(3,41)} = 2.15$; $P < 0.001$; two-way ANOVA). (**i**) A plot of the percentage of time spent for individual animals in search of a hidden platform in a targeting quadrant during the probe trial ($n = 11$ mice per group, $P < 0.001$; *t*-test). (**j**) Bar graphs show that the performances measured by number of foot faults during the rotarod test are comparable among groups. Data are reported as the mean ± s.e.m. ($n = 11$ mice per group). In (**d**–**j**), four groups of male mice at 180 ± 5 days of age were used: control/$ECII_{PN}^{ChR2+}$ (control) and AD/$ECII_{PN}^{ChR2+}$ (AD) mice with (TBS) or without (non-TBS) treatment. AD, Alzhemer's disease; EC, entorhinal cortex; PV, parvalbumin; TBS, theta burst stimulation.

compared with the AD/ECII$_{PN}^{ChR2-}$ mice (Supplementary Figure S7d).

We next recorded ECII$_{PN}$–CA1$_{PV}$ synaptic transmission in the slices from the control and AD mice treated with (control/TBS and AD/TBS) or without (control/non-TBS and AD/non-TBS) TBS. To exclude disturbances from other projections (that is, the ECII$_{PN}$–DG–CA3–CA1$_{PV}$ indirect pathway), we cut off the connections of CA3 cells in the hippocampus to the dentate gyrus (Figure 4b). We analyzed the mean amplitude of the evoked EPSCs in CA1$_{PV}$ via blue light illuminations of ECII$_{PN}$ (Figure 4c) and of the miniature EPSCs (Figure 4d) and demonstrated that TBS treatment did not alter synaptic transmission in the control mice but was effective for the reversal of the ECII$_{PN}$–CA1$_{PV}$ synaptic decline in the AD mice. We also examined the miniature inhibitory postsynaptic currents in CA$_{PN}$, which primarily reflect the release probability of inhibitory γ-aminobutyric acid transmitter from CA1$_{PV}$ to CA1$_{PN}$ (Supplementary Figures S8a and b) and the firing probability of action potentials in both CA1$_{PN}$ (Figure 4f) and CA1$_{PV}$ (Supplementary Figures 8Sc and d). We found that all parameters examined in the AD/TBS mice were identical to those in the control/TBS mice, suggesting that optogenetic activation of ECII$_{PN}$ in the AD mice via the TBS paradigm protects against the decay of the ECII$_{PN}$ synaptic inputs into CA1$_{PV}$ and hence restores the excitatory and inhibitory synaptic balance in CA1$_{PN}$ microcircuits (Figure 4g–i).

Next, we examined the structure of ECII$_{PN}$–CA1$_{PV}$ synapses in the AD mice with or without TBS treatment. At the presynaptic sites, the synaptophysin-immunoreactive terminals in the stratum lacunosum-moleculare, an afferent axon terminal zone of ECII$_{PN}$ in the CA1 hippocampus, were stained with an antibody against synaptophysin protein (Supplementary Figure S9a). Our data showed that the densities of synaptophysin-labeled terminals in the stratum lacunosum-moleculare region of AD mice at 180 ± 5 days of age were 33.8 ± 3.9% lower than in the age-matched controls. This reduction of excitatory synaptic terminals in the stratum lacunosum-moleculare region of the AD mice was completely rescued by TBS treatment (Supplementary Figure S9b). At the postsynaptic sites, the dendritic spines in the CA1$_{PN}$ were comparable between the groups (Supplementary Figure S9c), but the spine densities in the CA1$_{PV}$ of AD mice decreased by 28.5 ± 4.2% compared with those in age-matched controls (Supplementary Figure S9d). Following TBS treatment, the spine density in the CA1$_{PV}$ dendritic branches of the AD mice was restored to the level identical to that in control mice (Supplementary Figure S9e). Together, these data demonstrate that TBS treatment can rescue synaptic loss in AD mice.

Rescue of learning and memory defects in AD mice

We next determined whether the rescue of ECII$_{PN}$–CA1$_{PV}$ synaptic loss by TBS treatment intercepts spatial learning and memory decline in the AD mice. First, we examined place cell firings in freely moving mice. We found that the information density significantly increased in the TBS-treated AD/ECII$_{PN}^{ChR2+}$ mice (Figures 5a and b) and that the size of the place field became identical between AD/ECII$_{PN}^{ChR2+}$ mice and control/ECII$_{PN}^{ChR2+}$ mice (Figure 5c). Thus, TBS treatment improves the representation and the precise spatial firing in CA1$_{PN}$. We next performed a hidden version of the Morris water maze test and found that AD/ECII$_{PN}^{ChR2+}$ mice after TBS treatment exhibited better performance in all measured indexes (Figures 5d–i); the latency and swim length to reach a hidden platform during the training session (Figures 5d–g) and the percentage of time spent in search of a hidden platform in each quadrant during the probe trial (Figures 5h and i) were comparable between the AD/ECII$_{PN}^{ChR2+}$ mice and the control/ECII$_{PN}^{ChR2+}$ mice after TBS treatment. In the control mice, TBS treatment did not alter spatial learning and memory and had no effect on motor coordination based on the rotarod tests (Figure 5j), body weight (Supplementary Figure S10a) or motor activity based on the open-field tests (Supplementary Figures S10b and c). Thus, optogenetic activation of ECII$_{PN}$ with a TBS paradigm effectively promotes the recovery of spatial learning and memory decay without altering the learning and memory-unrelated functions in AD mice.

DISCUSSION

The present study explored the synaptic mechanisms underlying spatial learning and memory defects in the AD mice, with the following three key findings. First, we uncovered that ECII$_{PN}$ innervate to CA1$_{PV}$ via a direct pathway, and this pathway is selectively degenerated in an early stage of AD. Second, we delineated that the loss of ECII$_{PN}$–CA1$_{PV}$ synapses constitutes an essential cellular event for disease progression, such as memory loss, in an early stage of AD. Finally, we found that optogenetic activation of ECII$_{PN}$ via a TBS paradigm induces beneficial effects and effectively protects against synaptic and behavioral decays in the AD mice. Thus, the present work not only reveals the synaptic circuits of the ECII$_{PN}$–CA1$_{PV}$ pathway underlying impairments in spatial learning and memory but also provides a promising target for therapeutic intervention to treat disease progression in AD.

Previous studies suggested that both ECII$_{PN}$ and ECIII$_{PN}$ project their afferents to CA1$_{PN}$ through two independent pathways, including the trisynaptic or indirect pathway, in which ECII$_{PN}$ have synaptic connections directly to granule cells in the dentate gyrus,[14,17] and a direct pathway, in which ECIII$_{PN}$ have axon terminals that target CA1$_{PN}$.[15–17] However, sufficient evidence for the existence of such a direct ECIII$_{PN}$–CA1$_{PN}$ pathway is lacking. A recent study showed that island cells in the ECII, but not in the ECIII, project their axon terminals to CA1$_{IN}$.[20] However, several types of CA1$_{IN}$ have been identified, and which types of CA1$_{IN}$ receive excitatory synaptic inputs directly from ECII$_{PN}$ has yet to be studied. The present work provides compelling evidence (both anatomical and functional) showing a direct synaptic connection between the CA1$_{PV}$ subtype of CA1$_{IN}$ and ECII$_{PN}$. First, monosynaptic retrograde labeling showed that ΔG-rabies virus-mCherry is expressed in CA1$_{PV}^{TVA/G+}$ and ECII$_{PN}^{TVA/G-}$ neurons. Second, optogenetic activation of ECII$_{PN}$ reliably evokes EPSCs in CA1$_{PV}$ (only small synaptic responses in CA1$_{PN}$) with a latency in line with monosynaptic transmission. Third, optogenetic stimulation specifically targets ECII$_{PN}$ because it evokes action potentials in ECII$_{PN}$ but not in ECIII$_{PN}$. In addition, we created rAAV1/2-D28K-Cre virus particles to express ChR2 restrictively in the ECII$_{PN}$ of AD mice. These two independent experiments provide sufficient evidence showing that ECII$_{PN}$, but not ECIII$_{PN}$, directly innervate CA1$_{PV}$.

The present study included Morris water maze tests and place cell recordings to analyze spatial learning and memory. We found that AD mice (Tg2576) exhibited memory defects beginning at 180 days of age.[32,34,45] Several previous studies also examined the behavioral performance of AD mice in Morris water maze tasks. Some studies reported that the AD mice exhibited a spatial memory loss at 9–10 months of age[46,47] or after 14 months of age,[48,49] whereas other studies clarified that the AD mice exhibited impaired spatial learning and memory at 4–6 months of age.[50,51] One earlier study detected a memory loss in the AD mice as early as 3 months of age.[52] The discrepancies among these studies might be due to differences in experimental paradigms and the genetic background of the AD mice used in different laboratories. For example, some studies conducted training with nine trials per day for 6 days, whereas others applied 10 trials per day for 4 days. In addition, the genetic background of the AD mice might affect the outcome of the behavioral tests. In our study, the AD mice (Tg2576 but not APP/PS1, APP/PS1/Tau or 5XFAD mice) were crossed with ChR2 mice, PV-Cre mice with the C57BL/6 background. The mutant mice and the nontransgenic

controls were housed in the same conditions and derived from the same litters.

DBS has shown promise as a therapeutic intervention for some neurological disorders.[39] For example, DBS can mitigate symptoms in AD,[40] Parkinson's disease,[41] epilepsy[42] and depression.[43] DBS stimulations can produce beneficial effects in the brain, such as the release of transmitters and activity-dependent neurotrophins, such as brain-derived neurotrophic factor and nerve growth factor, that are required for neuronal cell survival and regeneration.[53–55] However, these conventional strategies are limited by imprecise activation or inhibition of brain cell types/circuits and hence generate severe deleterious effects, such as psychiatric, motor and speech problems.[56,57] The present study overcame these limitations of electrical stimulation. We developed an optogenetic strategy to selectively activate and/or inactivate the individual excitatory/inhibitory synapses in a specific group of neurons with millisecond-scale temporal precision in a manner similar to that used in brain neuronal firing patterns.[58,59] Thus, optogenetic stimulation is a promising strategy for AD therapy, as it does not generate obvious adverse effects *in vivo*.

CONFLICT OF INTEREST

The authors declare no conflict of interest.

ACKNOWLEDGMENTS

This work was supported by the National Natural Science Foundation of China (Grants: 81130079 to YL, 91232302 to YL, 91132725 to L-QZ, 31571039 to L-QZ and 81200863 to LP) and the Chinese Academy of Sciences (XDB02050500) and Top-Notch Young Talents Program of China of 2014, and Academic Frontier Youth Team of HUST to L-QZ. We sincerely thank Ms Na Wei (HUST) for behavioral analyses, Dr Hui-Juan Jin (HUST) for mice breeding and genotypes, Shan Wang (HUST) for western blot analysis and Dr Hengye Man (Boston University) for the comments on the manuscript.

AUTHOR CONTRIBUTIONS

YL, L-QZ and QT conceived and designed the studies and wrote the paper. XY, TT and CY performed optogenetics and electrophysiological studies. HL, JW and LP carried out behavioral analyses, immunohistochemistry and cell counting. LP supervised *in vivo* place cell recordings. XL, FX and DL constructed virus vectors and performed injections and imaging. All the authors contributed to the data analysis and presentation in the paper.

REFERENCES

1 Duffy AM, Morales-Corraliza J, Bermudez-Hernandez KM, Schaner MJ, Magagna-Poveda A, Mathews PM *et al.* Entorhinal cortical defects in Tg2576 mice are present as early as 2-4 months of age. *Neurobiol Aging* 2015; **36**: 134–148.
2 Gomez-Isla T, Price JL, McKeel DW Jr, Morris JC, Growdon JH, Hyman BT. Profound loss of layer II entorhinal cortex neurons occurs in very mild Alzheimer's disease. *J Neurosci* 1996; **16**: 4491–4500.
3 Jack CR Jr, Knopman DS, Jagust WJ, Shaw LM, Aisen PS, Weiner MW *et al.* Hypothetical model of dynamic biomarkers of the Alzheimer's pathological cascade. *Lancet Neurol* 2010; **9**: 119–128.
4 Chapman PF, White GL, Jones MW, Cooper-Blacketer D, Marshall VJ, Irizarry M *et al.* Impaired synaptic plasticity and learning in aged amyloid precursor protein transgenic mice. *Nat Neurosci* 1999; **2**: 271–276.
5 Hsia AY, Masliah E, McConlogue L, Yu GQ, Tatsuno G, Hu K *et al.* Plaque-independent disruption of neural circuits in Alzheimer's disease mouse models. *Proc Natl Acad Sci USA* 1999; **96**: 3228–3233.
6 Ittner LM, Ke YD, Delerue F, Bi M, Gladbach A, van Eersel J *et al.* Dendritic function of tau mediates amyloid-beta toxicity in Alzheimer's disease mouse models. *Cell* 2010; **142**: 387–397.
7 Arendt T. Synaptic degeneration in Alzheimer's disease. *Acta Neuropathol* 2009; **118**: 167–179.
8 Jacobsen JS, Wu CC, Redwine JM, Comery TA, Arias R, Bowlby M *et al.* Early-onset behavioral and synaptic deficits in a mouse model of Alzheimer's disease. *Proc Natl Acad Sci USA* 2006; **103**: 5161–5166.
9 Scheff SW, Price DA, Schmitt FA, DeKosky ST, Mufson EJ. Synaptic alterations in CA1 in mild Alzheimer disease and mild cognitive impairment. *Neurology* 2007; **68**: 1501–1508.
10 Zhou Y, Dougherty JH Jr, Hubner KF, Bai B, Cannon RL, Hutson RK. Abnormal connectivity in the posterior cingulate and hippocampus in early Alzheimer's disease and mild cognitive impairment. *Alzheimers Dement* 2008; **4**: 265–270.
11 Huijbers W, Mormino EC, Wigman SE, Ward AM, Vannini P, McLaren DG *et al.* Amyloid deposition is linked to aberrant entorhinal activity among cognitively normal older adults. *J Neurosci* 2014; **34**: 5200–5210.
12 Van Hoesen GW, Hyman BT, Damasio AR. Entorhinal cortex pathology in Alzheimer's disease. *Hippocampus* 1991; **1**: 1–8.
13 Yassa MA. Ground zero in Alzheimer's disease. *Nat Neurosci* 2014; **17**: 146–147.
14 Amaral D, Witter M. The three-dimensional organization of the hippocampal formation: a review of anatomical data. *Neurosci* 1989; **31**: 571–591.
15 Mcmenemey W. The structure of Ammon's horn. *J Neurol Neurosurg Psychiatry* 1969; **32**: 254.
16 Steward O, Scoville SA. Cells of origin of entorhinal cortical afferents to the hippocampus and fascia dentata of the rat. *J Comp Neurol* 1976; **169**: 347–370.
17 Witter M, Groenewegen H, Da Silva FL, Lohman A. Functional organization of the extrinsic and intrinsic circuitry of the parahippocampal region. *Prog Neurobiol* 1989; **33**: 161–253.
18 Brun VH, Leutgeb S, Wu HQ, Schwarcz R, Witter MP, Moser EI *et al.* Impaired spatial representation in CA1 after lesion of direct input from entorhinal cortex. *Neuron* 2008; **57**: 290–302.
19 Brun VH, Otnass MK, Molden S, Steffenach HA, Witter MP, Moser MB *et al.* Place cells and place recognition maintained by direct entorhinal-hippocampal circuitry. *Science* 2002; **296**: 2243–2246.
20 Kitamura T, Pignatelli M, Suh J, Kohara K, Yoshiki A, Abe K *et al.* Island cells control temporal association memory. *Science* 2014; **343**: 896–901.
21 Tu W, Xu X, Peng L, Zhong X, Zhang W, Soundarapandian MM *et al.* DAPK1 interaction with NMDA receptor NR2B subunits mediates brain damage in stroke. *Cell* 2010; **140**: 222–234.
22 Pei L, Shang Y, Jin H, Wang S, Wei N, Yan H *et al.* DAPK1–p53 interaction converges necrotic and apoptotic pathways of ischemic neuronal death. *J Neurosci* 2014; **34**: 6546–6556.
23 Pei L, Wang S, Jin H, Bi L, Wei N, Yan H *et al.* A novel mechanism of spine damages in stroke via DAPK1 and Tau. *Cereb Cortex* 2015; **25**: 4559–4571.
24 Wang X, Pei L, Yan H, Wang Z, Wei N, Wang S *et al.* Intervention of death-associated protein kinase 1–p53 interaction exerts the therapeutic effects against stroke. *Stroke* 2014; **45**: 3089–3091.
25 Ray S, Naumann R, Burgalossi A, Tang Q, Schmidt H, Brecht M. Grid-layout and theta-modulation of layer 2 pyramidal neurons in medial entorhinal cortex. *Science* 2014; **343**: 891–896.
26 Gunaydin LA, Yizhar O, Berndt A, Sohal VS, Deisseroth K, Hegemann P. Ultrafast optogenetic control. *Nat Neurosci* 2010; **13**: 387–392.
27 Kitamura T, Sun C, Martin J, Kitch LJ, Schnitzer MJ, Tonegawa S. Entorhinal cortical ocean cells encode specific contexts and drive context-specific fear memory. *Neuron* 2015; **87**: 1317–1331.
28 Sun C, Kitamura T, Yamamoto J, Martin J, Pignatelli M, Kitch LJ *et al.* Distinct speed dependence of entorhinal island and ocean cells, including respective grid cells. *Proc Natl Acad Sci USA* 2015; **112**: 9466–9471.
29 Varga C, Lee SY, Soltesz I. Target-selective GABAergic control of entorhinal cortex output. *Nat Neurosci* 2010; **13**: 822–824.
30 Busche MA, Chen X, Henning HA, Reichwald J, Staufenbiel M, Sakmann B *et al.* Critical role of soluble amyloid-beta for early hippocampal hyperactivity in a mouse model of Alzheimer's disease. *Proc Natl Acad Sci USA* 2012; **109**: 8740–8745.
31 Palop JJ, Mucke L. Epilepsy and cognitive impairments in Alzheimer disease. *Arch Neurol* 2009; **66**: 435–440.
32 Lesne S, Koh MT, Kotilinek L, Kayed R, Glabe CG, Yang A *et al.* A specific amyloid-beta protein assembly in the brain impairs memory. *Nature* 2006; **440**: 352–357.
33 Stewart S, Cacucci F, Lever C. Which memory task for my mouse? A systematic review of spatial memory performance in the Tg2576 Alzheimer's mouse model. *J Alzheimers Dis* 2011; **26**: 105–126.
34 Westerman MA, Cooper-Blacketer D, Mariash A, Kotilinek L, Kawarabayashi T, Younkin LH *et al.* The relationship between Aβ and memory in the Tg2576 mouse model of Alzheimer's disease. *J Neurosci* 2002; **22**: 1858–1867.
35 Langston RF, Ainge JA, Couey JJ, Canto CB, Bjerknes TL, Witter MP *et al.* Development of the spatial representation system in the rat. *Science* 2010; **328**: 1576–1580.
36 Moser EI, Kropff E, Moser MB. Place cells, grid cells, and the brain's spatial representation system. *Annu Rev Neurosci* 2008; **31**: 69–89.
37 O'Keefe J, Burgess N. Dual phase and rate coding in hippocampal place cells: theoretical significance and relationship to entorhinal grid cells. *Hippocampus* 2005; **15**: 853–866.

38 Sasaki T, Leutgeb S, Leutgeb JK. Spatial and memory circuits in the medial entorhinal cortex. *Curr Opin Neurobiol* 2015; **32**: 16–23.
39 Fregni F, Pascual-Leone A. Technology insight: noninvasive brain stimulation in neurology—perspectives on the therapeutic potential of rTMS and tDCS. *Nat Clin Pract Neurol* 2007; **3**: 383–393.
40 Kuhn J, Hardenacke K, Lenartz D, Gruendler T, Ullsperger M, Bartsch C *et al.* Deep brain stimulation of the nucleus basalis of Meynert in Alzheimer's dementia. *Mol Psychiatry* 2014; **20**: 353–360.
41 Moro E, Lang AE. Criteria for deep-brain stimulation in Parkinson's disease: review and analysis. *Expert Rev Neurother* 2006; **6**: 1695–1705.
42 Wu C, Sharan AD. Neurostimulation for the treatment of epilepsy: a review of current surgical interventions. *Neuromodulation* 2013; **16**: 10–24, discussion 24.
43 Schlaepfer TE, Bewernick BH, Kayser S, Madler B, Coenen VA. Rapid effects of deep brain stimulation for treatment-resistant major depression. *Biol Psychiatry* 2013; **73**: 1204–1212.
44 Hasselmo ME. What is the function of hippocampal theta rhythm?—Linking behavioral data to phasic properties of field potential and unit recording data. *Hippocampus* 2005; **15**: 936–949.
45 Kilgore M, Miller CA, Fass DM, Hennig KM, Haggarty SJ, Sweatt JD *et al.* Inhibitors of class 1 histone deacetylases reverse contextual memory deficits in a mouse model of Alzheimer's disease. *Neuropsychopharmacology* 2010; **35**: 870–880.
46 Hsiao K, Chapman P, Nilsen S, Eckman C, Harigaya Y, Younkin S *et al.* Correlative memory deficits, Abeta elevation, and amyloid plaques in transgenic mice. *Science* 1996; **274**: 99–102.
47 King DL, Arendash GW, Crawford F, Sterk T, Menendez J, Mullan MJ. Progressive and gender-dependent cognitive impairment in the APP(SW) transgenic mouse model for Alzheimer's disease. *Behav Brain Res* 1999; **103**: 145–162.
48 Mitchell JC, Perkinton MS, Yates DM, Lau KF, Rogelj B, Miller CC *et al.* Expression of the neuronal adaptor protein X11alpha protects against memory dysfunction in a transgenic mouse model of Alzheimer's disease. *J Alzheimers Dis* 2010; **20**: 31–36.
49 Quinn JF, Bussiere JR, Hammond RS, Montine TJ, Henson E, Jones RE *et al.* Chronic dietary alpha-lipoic acid reduces deficits in hippocampal memory of aged Tg2576 mice. *Neurobiol Aging* 2007; **28**: 213–225.
50 Holcomb LA, Gordon MN, Jantzen P, Hsiao K, Duff K, Morgan D. Behavioral changes in transgenic mice expressing both amyloid precursor protein and presenilin-1 mutations: lack of association with amyloid deposits. *Behav Genet* 1999; **29**: 177–185.
51 Lindner MD, Hogan JB, Krause RG, Machet F, Bourin C, Hodges DB *et al.* Soluble Aβ and cognitive function in aged F-344 rats and Tg2576 mice. *Behav Brain Res* 2006; **173**: 62–75.
52 King DL, Arendash GW. Behavioral characterization of the Tg2576 transgenic model of Alzheimer's disease through 19 months. *Physiol Behav* 2002; **75**: 627–642.
53 Fritsch B, Reis J, Martinowich K, Schambra HM, Ji Y, Cohen LG *et al.* Direct current stimulation promotes BDNF-dependent synaptic plasticity: potential implications for motor learning. *Neuron* 2010; **66**: 198–204.
54 Mattson MP. Glutamate and neurotrophic factors in neuronal plasticity and disease. *Ann N Y Acad Aci* 2008; **1144**: 97–112.
55 Schinder AF, Poo M. The neurotrophin hypothesis for synaptic plasticity. *Trends Neurosci* 2000; **23**: 639–645.
56 Blomstedt P, Hariz MI. Are complications less common in deep brain stimulation than in ablative procedures for movement disorders? *Stereotact Funct Neurosurg* 2006; **84**: 72–81.
57 Hariz MI. Complications of deep brain stimulation surgery. *Mov Disord* 2002; **17**: S162–S166.
58 Fenno L, Yizhar O, Deisseroth K. The development and application of optogenetics. *Annu Rev Neurosci* 2011; **34**: 389–412.
59 Kalanithi P, Henderson JM. Optogenetic neuromodulation. *Int Rev Neurobiol* 2012; **107**: 185–205.

Supplementary Information accompanies the paper on the Molecular Psychiatry website (http://www.nature.com/mp)